Short Article

Cell Stem Cell

Midbrain-like Organoids from Human Pluripotent Stem Cells Contain Functional Dopaminergic and Neuromelanin-Producing Neurons

Graphical Abstract

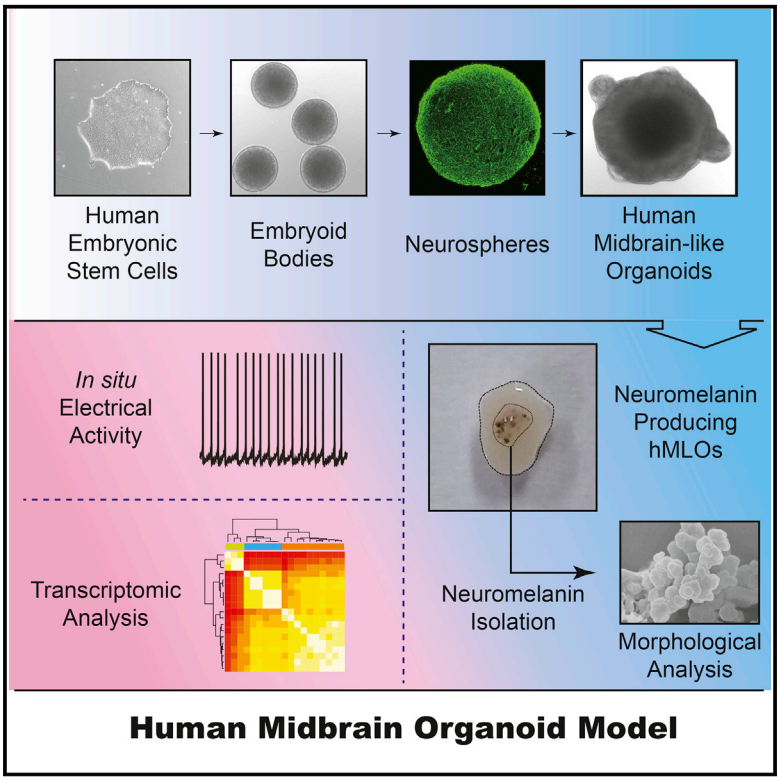

Highlights

- Self-organizing midbrain-like organoids (hMLOs) develop from hPSCs in 3D culture
- hMLOs, but not mouse MLOs or human cerebral organoids, produce neuromelanin
- hMLOs secrete dopamine (DA) and neurons within the hMLOs form functional synapses
- Neurons within hMLOs exhibit SNpc DA neuron-like electrophysiological properties

Authors

Junghyun Jo, Yixin Xiao, Alfred Xuyang Sun, ..., Eng King Tan, Hyunsoo Shawn Je, Huck-Hui Ng

Correspondence

shawn.je@duke-nus.edu.sg (H.S.J.), nghh@gis.a-star.edu.sg (H.-H.N.)

In Brief

Jo et al. report a method for generating human midbrain-like organoids (hMLOs) from hPSCs in 3D culture. The hMLOs contain distinct layers of neuronal cells expressing human midbrain markers, such as neuromelanin, are electrically active, form functional synapses, and produce dopamine, suggesting that they may be useful for studying human midbrain.

Accession Numbers

E-MTAB-4868

Jo et al., 2016, Cell Stem Cell *19*, 248–257
August 4, 2016
http://dx.doi.org/10.1016/j.stem.2016.07.005

CellPress

Cell Stem Cell
Short Article

Midbrain-like Organoids from Human Pluripotent Stem Cells Contain Functional Dopaminergic and Neuromelanin-Producing Neurons

Junghyun Jo,[1] Yixin Xiao,[2,3] Alfred Xuyang Sun,[1,4] Engin Cukuroglu,[1] Hoang-Dai Tran,[1,5] Jonathan Göke,[1] Zi Ying Tan,[1,6] Tzuen Yih Saw,[1] Cheng-Peow Tan,[1] Hidayat Lokman,[2] Younghwan Lee,[2] Donghoon Kim,[7] Han Seok Ko,[7] Seong-Oh Kim,[8] Jae Hyeon Park,[8] Nam-Joon Cho,[8,9] Thomas M. Hyde,[10,11,12] Joel E. Kleinman,[10,11] Joo Heon Shin,[10] Daniel R. Weinberger,[10,11,12,13,14] Eng King Tan,[4] Hyunsoo Shawn Je,[2,3,*] and Huck-Hui Ng[1,5,6,15,*]

[1]Genome Institute of Singapore, 60 Biopolis Street, Singapore 138672, Singapore
[2]Signature Program in Neuroscience and Behavioral Disorders, Duke-NUS Medical School, 8 College Road, Singapore 169857, Singapore
[3]Department of Physiology, Yong Loo Lin School of Medicine, National University of Singapore, Singapore 117597, Singapore
[4]National Neuroscience Institute, 20 College Road, Singapore 169856, Singapore
[5]Department of Biochemistry, National University of Singapore, 8 Medical Drive, Singapore 117597, Singapore
[6]Department of Biological Sciences, National University of Singapore, 14 Science Drive 4, Singapore 117543, Singapore
[7]Neuroregeneration and Stem Cell Programs, Institute for Cell Engineering, The Johns Hopkins University School of Medicine, Baltimore, MD 21205, USA
[8]School of Materials Science and Engineering, Nanyang Technological University, 50 Nanyang Avenue, Singapore 639798, Singapore
[9]KU-KIST Graduate School of Converging Science and Technology, Korea University, Seoul 136-701, Korea
[10]The Lieber Institute for Brain Development, 855 North Wolfe Street, Baltimore, MD 21205, USA
[11]Department of Psychiatry, Johns Hopkins University School of Medicine, Baltimore, MD 21205, USA
[12]Department of Neurology, Johns Hopkins University School of Medicine, Baltimore, MD 21205, USA
[13]Department of Neuroscience, Johns Hopkins University School of Medicine, Baltimore, MD 21205, USA
[14]McKusick-Nathans Institute of Genetic Medicine, Johns Hopkins University School of Medicine, Baltimore, MD 21205, USA
[15]School of Biological Sciences, Nanyang Technological University, 60 Nanyang Drive, Singapore 639798, Singapore
*Correspondence: shawn.je@duke-nus.edu.sg (H.S.J.), nghh@gis.a-star.edu.sg (H.-H.N.)
http://dx.doi.org/10.1016/j.stem.2016.07.005

SUMMARY

Recent advances in 3D culture systems have led to the generation of brain organoids that resemble different human brain regions; however, a 3D organoid model of the midbrain containing functional midbrain dopaminergic (mDA) neurons has not been reported. We developed a method to differentiate human pluripotent stem cells into a large multicellular organoid-like structure that contains distinct layers of neuronal cells expressing characteristic markers of human midbrain. Importantly, we detected electrically active and functionally mature mDA neurons and dopamine production in our 3D midbrain-like organoids (MLOs). In contrast to human mDA neurons generated using 2D methods or MLOs generated from mouse embryonic stem cells, our human MLOs produced neuromelanin-like granules that were structurally similar to those isolated from human substantia nigra tissues. Thus our MLOs bearing features of the human midbrain may provide a tractable in vitro system to study the human midbrain and its related diseases.

INTRODUCTION

The ability to make functional neural cells from human pluripotent stem cells (hPSCs) provides a unique opportunity to study human brain development and neurological disorders. Despite much progress, most protocols used to differentiate hPSCs into neurons are based on 2D methods that are unlikely to recapitulate the complexity and function of 3D in vivo neural circuits (Sasai, 2013). These limitations have prompted the development of 3D organoid models that mimic the organization and function of brain parts using hPSCs (Lancaster et al., 2013; Mariani et al., 2015; Muguruma et al., 2015; Paşca et al., 2015; Qian et al., 2016). In contrast to single-cell-type cultures, organoids consist of multiple cell types that self-organize spatially and can display enhanced cellular maturation and functionality, possibly due to the more appropriate 3D niche environment (Kelava and Lancaster, 2016).

Extensive research has focused on generating midbrain dopaminergic (mDA) neurons from hPSCs in recent years particularly because the selective loss of mDA neurons is a key pathological feature of Parkinson's disease (PD) (Grealish et al., 2014). Here, we report a method for differentiating hPSCs into human midbrain-like organoids (hMLOs) that recapitulate features of the midbrain and may be useful as a model for studying midbrain function and dysfunction.

RESULTS

Generation and Characterization of hMLOs from hPSCs

To generate midbrain organoids, we applied a guided self-organizing principle to hPSC culture. First, human embryonic stem cells (hESCs) were dissociated to single cells to form uniformly sized (approximately 400 μm in diameter) embryoid bodies (EBs) in low-attachment, V-shaped 96-well dishes (Figure 1A).

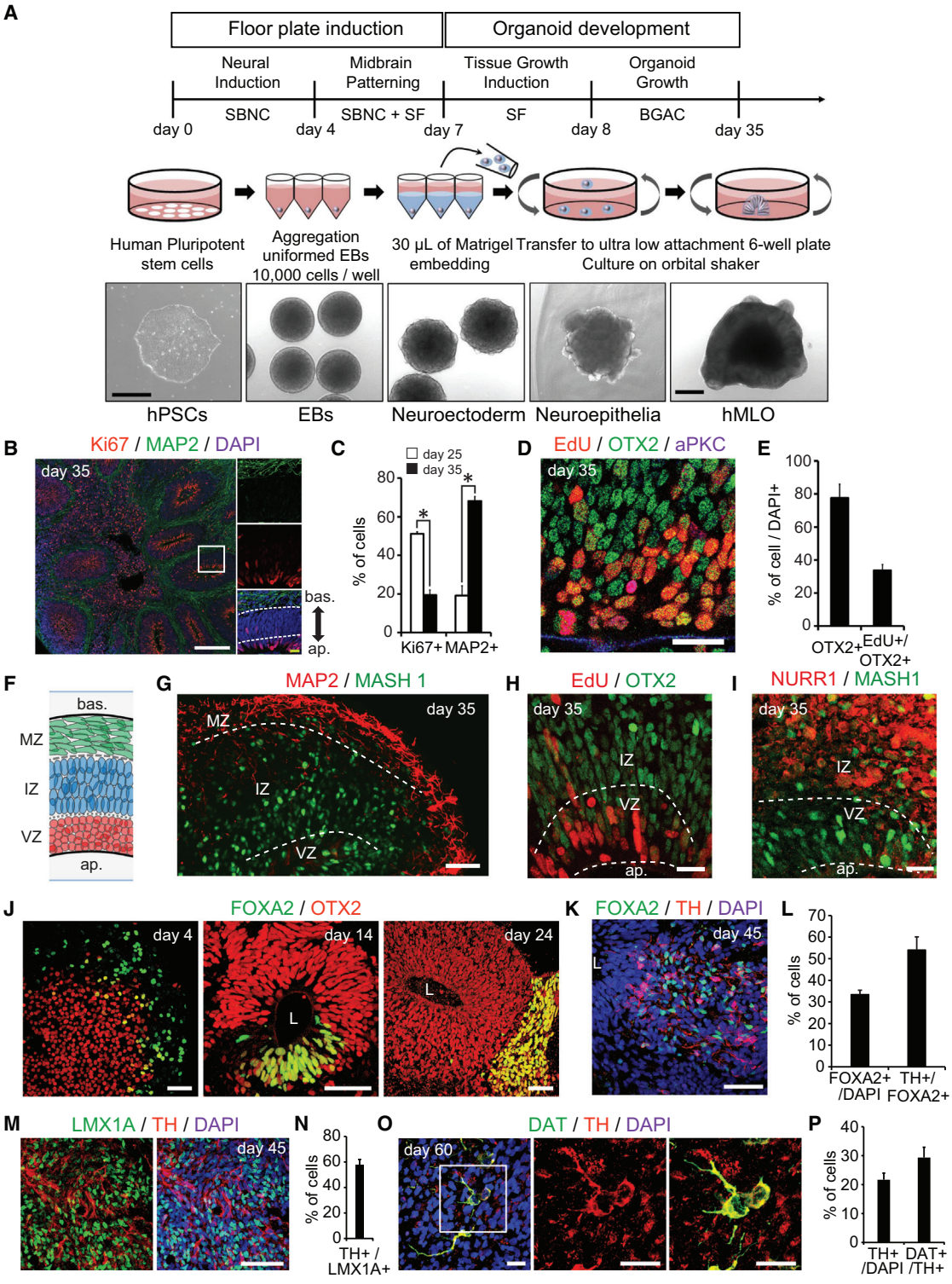

Figure 1. Generation and Characterization of hMLOs from hPSCs

(A) Schematic diagrams illustrating the overall strategy to generate hMLOs. Differential interface contrast (DIC) images illustrate the typical morphology of cells at each stage. SBNC: SB431542, Noggin, and CHIR99021; SF: SHH-C25II and FGF8; BGAC: BDNF, GDNF, ascorbic acid, and db-cAMP. Scale bars, 500 μm.

(B) Left: cryosection of an hMLO at day 35 stained for Ki67 and MAP2. Right: a zoom-in view of the white box. White scale bar, 200 μm. Yellow scale bar, 10 μm.

(C) Quantification of the percentage of Ki67$^+$ and MAP2$^+$ cells at day 25 and 35 hMLOs by FACS analysis. Error bars represent mean ± SEM (n = 3, *p < 0.05, Student's t test).

(D) Immunostaining of EdU, OTX2, and aPKC at the apical region of a neuroepithelium (NE). Scale bar, 20 μm.

(legend continued on next page)

To promote neuroectodermal differentiation toward a floor plate, these EBs were simultaneously treated with dual-SMAD inhibition factors (Noggin and SB431542) and a Wnt pathway activator (CHIR99021). The resulting EBs were patterned toward a mesencephalic fate upon addition of sonic hedgehog (SHH) and FGF8 (Arenas, 2014; Chambers et al., 2009; Kirkeby et al., 2012) (Figure 1A). At day 7, nascent neural organoids expressed markers of mDA progenitors such as *FOXA2*, *OTX2*, *CORIN*, and *LMX1A* (Figure S1A). Subsequently, each neuroectodermal spheroid was embedded in Matrigel to promote growth and organization in 3D (Figure 1A) and then transferred to a tissue culture plate containing neuronal media supplemented with neurotrophic factors (Figure 1A). The organoids were cultured in this manner on an orbital shaker until the day of analysis. These neural organoids grew to more than 2 mm in diameter in 30 days and contained multiple neuroepithelia (Figures 1A, S1B, and S1C). Immunohistochemical analysis revealed that these neuroepithelia exhibited apical-basal polarity based on the localization of atypical protein kinase C (aPKC) (Figures S1D and S1E). $Ki67^+$ proliferating cells and $MAP2^+$ neurons were detected at the apical and the basal surface, respectively (Figure 1B). FACS analysis revealed that the percentage of $Ki67^+$ cells decreased from 51% at day 25 to 19% at day 35; conversely, the proportion of $MAP2^+$ cells increased 3.6-fold (Figure 1C). These data indicate that cells in the hMLOs gradually transitioned from proliferating neuroprogenitors to post-mitotic mature neurons. To further characterize the developing midbrain neuroepithelia, we labeled proliferating progenitor cells with EdU and stained for OTX2, a transcription factor that separates the midbrain from the hindbrain. OTX2 expression was observed in cells within the apical surface and extended to the intermediate region of the neuroepithelia (Figure 1D). Approximately 80% of all cells were $OTX2^+$ and 35% of the cells within neuroepithelia were double positive for EdU and OTX2 (Figure 1E), demonstrating that proliferating cells near the apical region of hMLOs were midbrain progenitors.

Next, we examined the cytoarchitecture of the neural organoids at day 35. Similar to the layering of the murine embryonic midbrain floor plate that eventually gives rise to mDA neurons (Baizabal and Covarrubias, 2009), the hMLOs at day 35 showed three layers: the proliferative ventral zone (VZ), where neural progenitors reside; the intermediate zone (IZ), which immature mDA neurons pass through as they migrate ventrally; and the mantle zone (MZ), where maturing mDA neurons begin to express genes associated with the synthesis of dopamine (DA) (Figure 1F). In the VZ and IZ, the midbrain progenitors expressed MASH1 and OTX2 (Figures 1G and 1H). We also detected the orphan nuclear receptor NURR1, which is expressed in post-mitotic mDA progenitors, in the IZ (Figure 1I) (Arenas et al., 2015). These data suggest that the features of our in vitro hMLOs are similar to those of early in vivo midbrains in the aspect of developing neuroectoderm toward floor plate.

Identification and Verification of mDA Neurons in hMLOs

Several studies have demonstrated that FOXA2, a floor plate marker, identifies neuronal progenitors that eventually become mDA neurons (Sasaki et al., 1997). We observed FOXA2 expression in developing hMLOs as early as day 4 (Figure 1J). Intriguingly, at day 14, FOXA2 expression became restricted to specific domains within the neuroepithelia, and by day 24, FOXA2-expressing cells presumably had migrated radially to the MZ (Figure 1J), where they began to express tyrosine hydroxylase (TH), a defining marker of DA neurons. Indeed at day 45 the majority of $FOXA2^+$ cells (54%) also expressed TH (Figures 1K and 1L). Given that some ventral forebrain progenitors could also express FOXA2 (Liu and Zhang, 2011), we sought to examine the expression of other mDA neuroprogenitor markers such as LMX1A and OTX2 together with FOXA2 in the hMLOs at day 14 and 45. We observed that 22% of cells at day 14 were double positive for LMX1A and OTX2 (Figures S1F and S1G). At day 45, 38% of all cells were $LMX1A^+$, and most of them (81%) were also $FOXA2^+$ (Figures S1H and S1I). We further observed that a major fraction of $LMX1A^+$ cells (58%) expressed TH at this time (Figures 1M and 1N). These data strongly suggest that the majority of TH^+ neurons in the hMLOs likely originated from $FOXA2^+$ and $LMX1A^+$ progenitors, which were a subset of $OTX2^+$ cells. In addition, we observed robust expression of the mDA markers in hMLOs by qPCR (Figure S1J). Taken together, these data demonstrated a time-dependent induction of floor plate precursors and their subsequent differentiation into TH^+ mDA neurons within the developing hMLOs.

To further quantify the neuronal populations within the hMLOs, we conducted FACS analysis. At day 35, 6% of the $MAP2^+$ neurons in hMLOs co-expressed TH, and the number increased significantly to 22% by day 60 (Figures S1K–S1M). Approximately 29% were also positive for DA transporter (DAT) (Figures 1O and 1P). Intriguingly, at day 60, we observed that some of the TH^+ neurons were also positive for GIRK2 (G protein-gated inwardly rectifying K^+ channel 2), which is an important protein with enriched expression in A9 subtype mDA neurons (Figure S1N). In addition, we observed occasional cells double-positive for TH and Calbindin, suggesting that they are likely to be

(E) Percentages of $OTX2^+$ and OTX^+/EdU^+ cells at the apical region of an NE. Error bars represent mean ± SEM (n = 7).
(F) Schematic of the laminar structure in the hMLOs (bas., basal; ap., apical; MZ, mantle zone; IZ, intermediate zone; VZ, ventral zone).
(G) Cryosection of a day 35 hMLO stained for MAP2 and MASH1. Scale bar, 50 μm.
(H) EdU labeling and OTX2 immunostaining of a day 35 hMLO. Scale bar, 20 μm.
(I) Cryosection of a day 35 hMLO stained for NURR1 and MASH1. Scale bar, 20 μm.
(J) Cryosection of an hMLO at days 4, 14, and 24 stained for FOXA2 (floor plate progenitors) and OTX2 (midbrain intermediate progenitors) (L, lumen). Scale bars, 50 μm.
(K and L) Immunostaining of FOXA2 and TH of an hMLO at day 45 (K). Scale bars, 50 μm (L, lumen). The quantifications are shown in (L). Error bars represent mean ± SEM (n = 3).
(M and N) Cryosection of a day 45 hMLO labeled for LMX1A and TH (M). Scale bars, 50 μm. The quantification is shown in (N). Error bars represent mean ± SEM (n = 3).
(O and P) Immunostaining of MZ cells at day 60 with DAT and TH antibodies, zoom-in view to illustrate some cells double positive for DAT and TH (O). The quantifications are shown in (P). Error bars represent mean ± SEM (n = 3). Scale bar, 20 μm.
See also Figure S1.

A10-like subtype mDA neurons (Figure S1O). In sum, these data suggest that our neural organoids, after long-term culturing, produced A9-like mDA neurons which expressed TH, DAT, and GIRK2.

Transcriptional Characterization of hMLOs

While the hMLOs consist of DA neurons that are typical of midbrain tissue, the cellular heterogeneity and structure of the organoid culture might allow us to model aspects that cannot be studied using 2D culture. To investigate this hypothesis, we generated gene expression profiles for our organoid model system and 2D-grown mDA neurons (Figures S2A–S2D). Indeed, a large number of genes show differential expression between hMLOs and 2D-DA neurons (Figure 2A, Table S1). To test if the differences of hMLOs and 2D-DA neurons in transcriptomes reflect an upregulation of genes characteristic of brain development, we performed RNA-seq analyses from 10 human prenatal midbrain samples. A cluster analysis using the differentially expressed genes between hMLOs and 2D-DA neurons suggest that the hMLOs indeed show upregulation of genes that are expressed in human prenatal midbrain samples (Figure 2B). The genes that are differentially expressed in hMLOs compared to 2D-DA neurons significantly overlapped with differentially expressed genes in prenatal midbrain compared to 2D-DA neurons (Figures 2C, 2D, and S2E and Table S2, decreased expression: $p = 2.2e{-}248$; increased expression: $p = 4.13e{-}313$). Among the genes, which are expressed in hMLOs and prenatal midbrain, but not in 2D-DA neurons, were those genes expressed in additional cell types, such as *OLIG3* (oligodendrocyte gene) and *SLC1A3* (glial cell gene) (Figure 2E). mDA neuron-specific genes were commonly expressed in all samples (Figure 2F). A comparison with publicly available 2D-DA neuron expression data (Lin et al., 2016) and data from adult midbrain, forebrain, and hindbrain (Consortium, 2015) further suggests that hMLOs are closer to prenatal midbrain (Figure S2F). Together, this analysis of transcriptome profiles indicates that hMLOs indeed resemble aspects of gene expression profiles of prenatal midbrain that appear to be absent from mDA neurons generated by the conventional 2D method.

Identification of Neuromelanin and A9-like mDA Neurons in Human MLOs

During the long-term culture of the hMLOs, we observed sparse, black/brown-colored deposits in hMLOs by light microscopy after approximately 2 months. Furthermore, the number of these deposits gradually increased over time (Figure 3A). We hypothesized that these dark deposits were neuromelanin (NM), which are insoluble, black/brown granular pigments that accumulate in the substantia nigra pars compacta (SNpc) in humans and primates (Sulzer et al., 2000). To test this hypothesis, we performed Fontana-Masson staining and found that these deposits stained positive (Figures 3B and S3A). As shown in Figure 3B, large, rough, and darkly stained granules were observed within the neuronal cytosol, which were similar to the stained granules in human postmortem SNpc sections (Figure 3C). Some of these granules in the hMLOs could be observed outside of neuronal cells, indicating that these NM granules could be secreted from mDA neurons within the hMLOs (Figure 3B). In contrast, we failed to detect Fontana-Masson-positive granules from 2D-DA neurons (Kriks et al., 2011) (data not shown) or human cerebral organoids (hCOs) (Figures S3B and S3C) grown at a comparable number of days in vitro. Over time the amount of NM granules increased drastically (Figure 3D). Importantly, scanning electron microscopy and atomic force microscopy (AFM) revealed that NM granules isolated from the hMLOs exhibited similar morphological characteristics as those isolated from human postmortem SNpc tissue (Figures 3E and 3F, Figures S3D–S3F, and Table S3).

Given that NM is a byproduct of DA synthesis in mDA neurons, the addition of an exogenous dopamine precursor (L-DOPA) or DA is expected to accelerate the accumulation of NM in younger hMLO (Fedorow et al., 2005). Indeed, we observed a robust distribution of NM-like granules in the hMLOs at day 45 following a 10-day treatment of L-DOPA (50 μM) or DA (50 μM), whereas no NM-like granules were observed in untreated hMLOs or L-DOPA-treated hCOs (Figures 3G and S3G). To determine whether the NM-containing cells were TH^+, we immunostained adjacent sections from the same hMLO and observed TH^+ cells within the same area that displayed NM-like granules (Figure 3H). NM-like granules have been observed primarily in primates, but not in mice (Fedorow et al., 2005). Intriguingly, no NM-like granules were observed in mouse ESC-derived MLOs (mMLOs) that contained TH^+ neurons (Figure 3H). These data indicated that only human mDA neurons grown in 3D could produce NM-like granules in situ.

To further characterize the NM-containing mDA neurons, we reasoned that NM-containing cells should be an enriched population of A9 mDA neurons that are present in SNpc, and we thus used FACS to sort out NM-containing cells from hMLOs (Figures S3H and S3I). With this method, we could prospectively isolate NM^+ cells in the hMLOs (approximately 7% of total cells) (Figures S3J and S3K). We confirmed that isolated NM-containing cells were enriched with mDA neurons by immnostaining replated NM^+ cells with antibodies against MAP2 and TH (Figure S3L).

We performed reverse-transcription-specific target amplification on individual NM^+ sorted cells and noted that the vast majority of NM-sorted cells (87%) expressed MAP2, but among these cells some were negative for TH (Figure S3M), possibly due to the uptake of extracellularly released NM granules by non-dopaminergic neurons. We then focused our analysis on $TH^+/MAP2^+$ cells and characterized their subtype identity by the Fluidigm Biomark Array. Not surprisingly, most cells expressed pan-DA neuronal markers including EN1/2 (Figure S3N). We also noted that SNpc-related genes were more highly expressed in NM-containing cells, compared to ventral tegmental area (VTA)-related genes (Figure S3N) (Poulin et al., 2014), consistent with the known association of NM with A9, but not A10, neurons. Expression of markers indicative of other neuronal lineages was largely absent (Figure S3O). Collectively, these data indicate that the NM-containing neurons in the hMLOs preferentially expressed markers of SNpc, but not VTA, which corroborates well with our immunostaining data (Figure 1).

Functional Maturation of Dopaminergic Neurons in hMLOs

To test whether the neurons in the hMLOs were electrically active and functionally mature, we sliced hMLOs into 350 μm sections and performed acute, targeted, whole-cell patch recordings

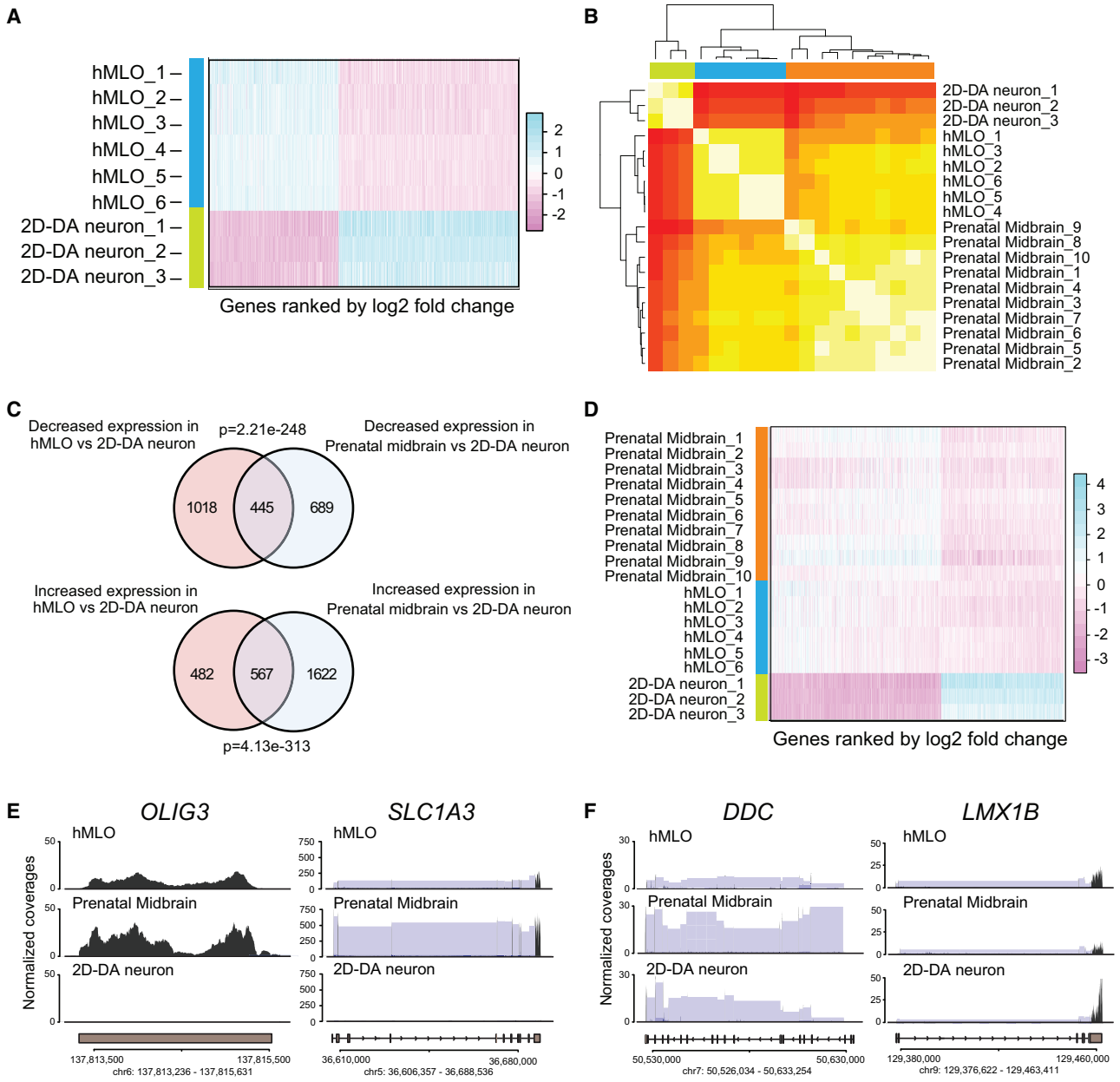

Figure 2. Transcriptional Characterization of hMLOs

(A) Heatmap showing differentially expressed genes between 2D-DA neurons and hMLOs, sorted by fold change (related to Table S1).

(B) Heatmap and clustering of expression data from 2D-DA neurons, hMLOs, and prenatal midbrain. The correlation of normalized gene expression using differentially expressed genes between 2D-DA neurons and hMLOs was used to estimate the distance between samples.

(C) Venn diagram indicating the overlap of genes that show upregulation or downregulation in hMLOs and prenatal midbrain compared to 2D-DA neurons (significance was estimated using Fisher's exact test).

(D) Heatmap showing genes that are differentially expressed between 2D-DA neurons and hMLOs and human prenatal midbrain, sorted by fold change (related to Table S2).

(E and F) Example genes expressed in prenatal midbrain and hMLOs, but not in 2D-DA neurons (E), and example genes commonly expressed in prenatal midbrain, hMLOs, and 2D-DA neurons (F). Black: normalized read count, blue: split reads that map to two exons. Shown is the average across all samples. See also Figure S2.

(Figure 4A) (Paşca et al., 2015; Yuan et al., 2015). In voltage-clamp mode, neurons within the hMLOs showed fast, inactivating inward and outward currents, which likely corresponded to the opening of voltage-dependent sodium (Na^+) and potassium (K^+) channels, respectively (Figure 4B). The peak voltage-gated Na^+- and K^+-channel currents increased significantly from day 33 to day 65 (Figure 4C). Consistently, we observed a considerable decrease in membrane resistance (Rm) and increase in

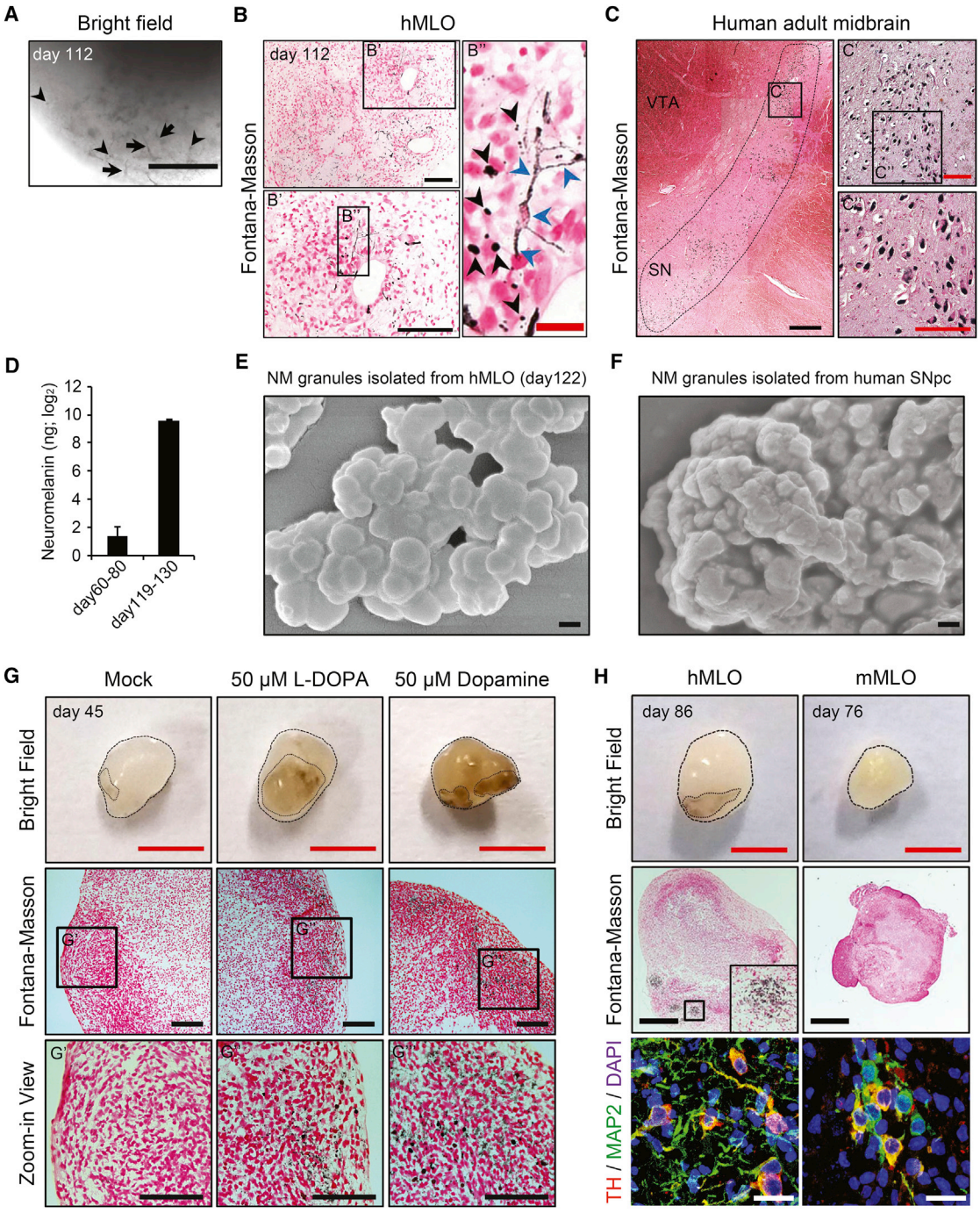

Figure 3. Identification of Neuromelanin in hMLOs

(A) Appearance of dark granules in hMLOs at day 112. Note that dark pigments were localized within the neuronal compartment (arrows) as well as the extracellular compartment (arrowheads). Scale bar, 200 μm.

(B) Fontana-Masson staining to reveal neuromelanin (NM)-like granules within an hMLO. Note the presence of NM-like granules in both intracellular and extracellular compartments (blue and black arrowheads, respectively). Black scale bars, 100 μm. Red scale bar, 20 μm. (B′) is an enlarged view of a region in (B). (B″) is an enlarged view of a region in (B′).

(C) Fontana-Masson staining of human postmortem midbrain tissue. Black scale bars, 1 mm. Red scale bar, 200 μm. (C′) is an enlarged view of a region in (C) made from tiling multiple images of a large area. (C″) is an enlarged view of a region in (C′).

(D) NM content measurement in hMLOs. Error bars represent mean ±SEM (n = 3, respectively).

(E and F) SEM image of isolated NM granules (E) in a day 122 hMLO and (F) in human postmortem midbrain tissue (see also Figures S3D–S3F and Table S3). Scale bar, 200 nm.

(legend continued on next page)

membrane capacitance (Cm), and these changes correlated with the functional maturation of the neurons (Table S4). Action potentials (APs) were elicited when we depolarized the membrane in current-clamp mode (Figure 4D) and APs could be elicited from the majority of hMLO neurons (69.23%, n = 26) (Figure 4E and Table S4). Next, we investigated whether neurons within the hMLOs exhibited spontaneous synaptic transmission in situ, and we found that most of the recorded neurons showed spontaneous excitatory postsynaptic currents (sEPSCs) as well as spontaneous inhibitory postsynaptic currents (Figure 4F). In addition, we observed large-amplitude excitatory postsynaptic potentials (EPSPs > 20 pA) in response to extracellular electrical stimulation, demonstrating that the neurons inside the hMLOs participated in network activity (Figure 4G). More than 20% of neurons within the hMLOs showed rhythmic discharges, with an average frequency of 2.78 Hz (Figures 4H and 4I), and rebound depolarizations resulted in AP generation after short hyperpolarization of neurons (Figure 4J), which are characteristics of mDA neurons (Pfisterer et al., 2011). The application of the specific D2/D3 receptor agonist quinpirole (1 μM) markedly suppressed the firing of recorded neurons (Figures 4K and 4L), indicating the presence of functional dopamine receptors in mDA neurons within the hMLOs. Intriguingly, post hoc immunohistochemistry of the recorded neurons (labeled with biocytin) in the hMLOs revealed that most (n = 8/10) were TH^+, indicating that the recorded neurons were indeed mDA neurons (Figure 4M). Furthermore, high-performance liquid chromatography (HPLC) measurements showed that the DA content within hMLOs gradually increased as they matured (Figure 4N). Taken together, these data indicate that mDA neurons within the hMLOs produced DA, exhibited mature neuronal properties, and were able to form synapses with other neurons within the hMLOs.

DISCUSSION

Here, we have demonstrated that hESCs can be steered to differentiate into midbrain progenitors, which subsequently self-organize into 3D hMLOs comprising distinct cell layers with functional mDA neurons, but not the forebrain or the hindbrain (Figures S2G and S2H). Most approaches that have been developed so far have utilized 2D monolayer cultures on flat and rigid substrates to differentiate hPSCs into mDA neurons (Arenas et al., 2015). Although 2D cell culture has proven to be a valuable method for cell-based studies, lack of the 3D environment and multiple cell types has often led to inaccurate cellular responses and failure to recapitulate important physiological features of tissue in vivo (Fatehullah et al., 2016).

TH^+ neurons in the hMLOs exhibited biochemical and electrophysiological properties of mature mDA neurons and expressed functional DA receptors (Figures 4K and 4L). Intriguingly, these neurons receive inputs from other neuronal cells in the hMLOs, indicating that they make functional neuronal networks, demonstrating the potential utility of the hMLO in evaluating the degree of synaptic competence and connections. In our hMLOs, we observed other neuronal cells such as $GABA^+$ neurons (Figure S2I), consistent with in vivo midbrain (Korotkova et al., 2004). Although our transcriptome analysis showed that the hMLOs resemble prenatal midbrain and mDA neurons, future studies using single-cell transcriptome analysis may be required to further validate the similarity of the genetic expression program among them (Camp et al., 2015).

Strikingly, we found that human mDA neurons within 3D MLOs could produce NM-like granules while human mDA neurons in 2D culture and mouse mDA neurons within 3D MLOs did not. NM is a dark, complex, and insoluble pigment particularly concentrated in the mDA neurons of SN and in the noradrenergic neurons of locus coeruleus, the two brain areas mostly affected by PD (Fedorow et al., 2005). The origin and physiological function of NM remain controversial: several lines of evidence have demonstrated possible protective features of NM; however, many other studies concluded that NM is a toxic byproduct of DA synthesis in mDA neurons (Zecca et al., 2003) and that NM may trigger immune activation in the PD patient's brain (Zhang et al., 2011). The paucity of knowledge of NM has been due to the limited availability/accessibility of human NM, which could only be extracted from human postmortem midbrain tissues. Given the robustness of our protocol to generate human mDA neurons that readily produce NM granules, our 3D hMLOs provide a source of human DA neuron-derived NM in situ. Thus our method offers a potentially useful approach to study NM granules and associated proteins from PD patient-derived iPSC lines, which may shed light onto the underlying pathophysiological mechanisms of PD.

EXPERIMENTAL PROCEDURES

Cell Culture and Generation of hMLOs

The hESC lines H1 (WA01) and H9 (WA09) were cultured feeder-free on Matrigel (BD Biosciences) with mTeSR1 (StemCell Technologies, Inc.). hPSC lines before passage 40 were used to generate hMLOs. The hPSCs were dissociated to single cells to form uniform EBs in neuronal induction medium supplemented with 10 μM ROCK inhibitor Y27632 (Calbiochem). On day 4, hMLOs were cultured with the addition of midbrain patterning factors, 100 ng/mL SHH-C25II (R&D Systems) and 100 ng/mL FGF8 (R&D Systems) for 3 days. When neuroectodermal buds were starting to extrude, the hMLOs were embedded in 30 μL of reduced growth factor Matrigel and grown in tissue growth induction medium containing 100 ng/mL SHH-C25II and 100 ng/mL FGF8. After 24 hr, the hMLOs were embedded in Matrigel, transferred into ultra-low-attachment 6-well-plates (Costar) containing the final organoid differentiation media, which was supplemented with 10 ng/mL BDNF (Peprotech), 10 ng/mL GDNF (Peprotech), 100 μM ascorbic acid (Sigma-Aldrich), and 125 μM db-cAMP (Sigma-Aldrich), and cultured using an orbital shaker. The medium was replenished every 3 days. A detailed protocol of generating hMLOs is described in the Supplemental Experimental Procedures.

Human Brain Dissection

The ventral half of the midbrain was dissected from second trimester prenatal brainstem under visual inspection using a scalpel and hand-held dental drill (Table S5). Cases were donated with informed consent of the mother and

(G) The formation of NM-like granules was accelerated by L-DOPA (50 μM) and DA (50 μM) treatments. Red scale bar, 2 mm. Black scale bar, 100 μm. (G′), (G″), and (G‴) are high-magnification images of the black rectangle.
(H) NM-like granules were not observed in murine MLOs. Note that both the hMLO and mMLOs contain TH^+ mDA neurons (bottom panels). Red scale bar, 2 mm. Black scale bar, 500 μm. White scale bar, 20 μm.
See also Figure S3.

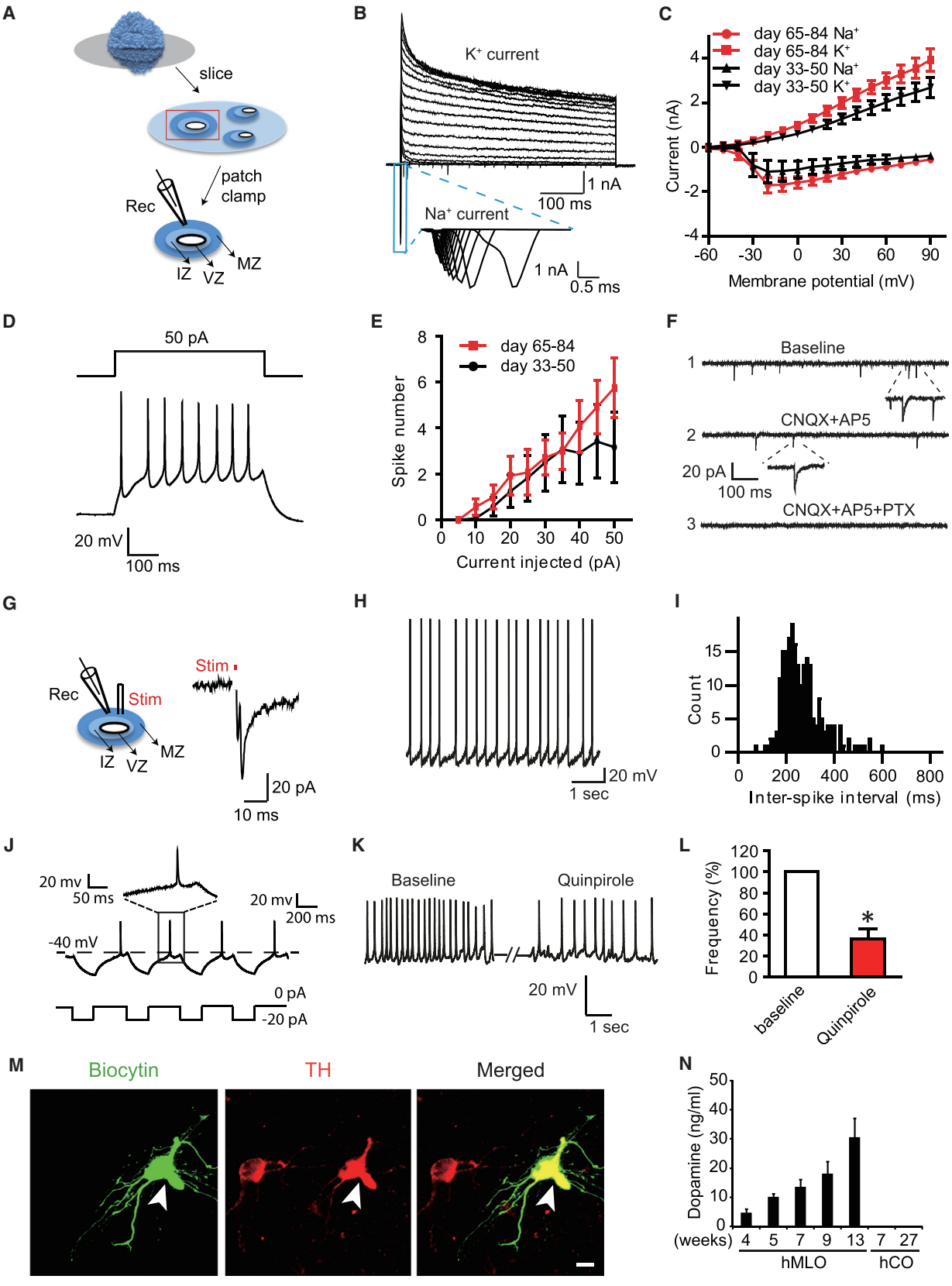

(legend on next page)

were selected on the basis of (1) the absence of any congenital anatomical abnormality upon macroscopic brain inspection and (2) the absence of any major genetic defect noted on prenatal testing. The IRB approval is from the Western IRB (study number, 1126332; WIRB protocol number, 20111080).

Immunohistochemistry and NM Staining

Immunohistochemistry of all organoids and tissue samples was performed as described in the Supplemental Experimental Procedures. Fontana-Masson staining to detect NM was performed according to the manufacturer's protocol. A detailed description is available in the Supplemental Experiment Procedures.

RNA Sequencing and Bioinformatics Analysis

RNA-seq was performed using hMLOs, 2D-DA neurons, or postmortem midbrain tissues (Table S5). For RNA-seq analysis, reads were mapped with TopHat2-2.0.12 (Kim et al., 2013), reads were counted using the R package GenomicAlignments (Lawrence et al., 2013), and differential expression was calculated using DESeq2 (Love et al., 2014). A detailed description is available in the Supplemental Experiment Procedures.

Electrophysiology

Excitability and synaptic transmission of neurons within hMLOs were studied by whole-cell patch clamp in either voltage- or current-clamp mode. See also Supplemental Experimental Procedures.

ACCESSION NUMBERS

The accession number for the RNA-seq data reported in this paper is E-MTAB-4868.

SUPPLEMENTAL INFORMATION

Supplemental Information for this article includes three figures, five tables, and Supplemental Experimental Procedures and can be found with this article online at http://dx.doi.org/10.1016/j.stem.2016.07.005.

AUTHOR CONTRIBUTIONS

J.J. conceived, designed, and conducted experiments and analyzed data; Y.X. performed electrophysiological recordings; H.D.T. and A.X.S. contributed idea and experimental design; E.C. and J.G. analyzed RNA-seq data; Z.Y.T performed flow cytometry analysis; H.D.T. and T.Y.S. cultured 2D-DA neurons; C.P.T. performed histological experiments; H.L. and Y.L. performed HPLC experiments; D.K. and H.S.K. isolated NM from human postmortem midbrain and provided postmortem human midbrain tissue slices; S.O.K., J.H.P., and N.J.C. performed scanning electron microscopy and AFM imaging and analyzed data; T.M.H. and J.E.K. provided human brain tissue and performed dissection; J.H.S. and D.R.W. performed RNA-seq on human prenatal midbrain; E.K.T. provided reagents; and E.K.T., H.S.J., and H.H.N. supervised the project. J.J., A.X.S., J.G., H.S.J., and H.H.N. wrote the paper. Y.X., A.X.S., and E.C. contributed equally to this study.

ACKNOWLEDGMENTS

We thank K.L. Lim and C. Chou for generously sharing reagents. We thank K.A. Gonzales, Y.S. Chan, and Y.S. Lim for assistance with experiments and intellectual discussion. We also thank O. Pletnikova and J. Troncoso for generously providing postmortem midbrain tissue samples. This work was supported by the Singapore Ministry of Education Academic Research Fund (MOE2012-T2-1-021), an Agency for Science, Technology and Research (A*STAR) Translational Collaborative Research Partnership Grant (TCRP, 13/1/96/688), a Duke-NUS Signature Research Program Block Grant (to H.S.J.), a National Medical Research Council Translational and Clinical Flagship grant (E.K.T. and H.H.N.), and A*STAR (H.H.N.). This work was also supported by grants from the NIH (NS082205 and NS38377) and the Maryland Stem Cell Research Foundation (RFA-MD-13-2). The authors acknowledge the joint participation by the Adrienne Helis Malvin Medical Research Foundation and the Diana Helis Henry Medical Research Foundation through its direct engagement in the continuous active conduct of medical research in conjunction with The Johns Hopkins Hospital, the Johns Hopkins University School of Medicine, the Foundation's Parkinson's Disease Program H-1, H-2013.

Received: November 30, 2015
Revised: April 22, 2016
Accepted: July 8, 2016
Published: July 28, 2016

REFERENCES

Arenas, E. (2014). Wnt signaling in midbrain dopaminergic neuron development and regenerative medicine for Parkinson's disease. Journal of Molecular Cell Biology *6*, 42–53.

Arenas, E., Denham, M., and Villaescusa, J.C. (2015). How to make a midbrain dopaminergic neuron. Development *142*, 1918–1936.

Baizabal, J.M., and Covarrubias, L. (2009). The embryonic midbrain directs neuronal specification of embryonic stem cells at early stages of differentiation. Dev. Biol. *325*, 49–59.

Camp, J.G., Badsha, F., Florio, M., Kanton, S., Gerber, T., Wilsch-Bräuninger, M., Lewitus, E., Sykes, A., Hevers, W., Lancaster, M., et al. (2015). Human

Figure 4. Functional Characterization of Dopaminergic Neurons from hMLOs

(A) Schematic diagram illustrating the experiment to investigate the electrophysiological activity of hMLOs in situ. Rec., recordings; Stim., electric stimulation.
(B) Representative traces showing the presence of voltage-dependent Na^+ and K^+ currents in neurons inside hMLOs. The blue box highlights Na^+ channel-dependent inward currents.
(C) Averaged current-voltage relationship (I/V) curves for the Na^+ and K^+ currents recorded. Error bars represent mean ± SEM (n = 12 and 14 for days 33–50 and 65–84, respectively).
(D) Representative traces of multiple APs (the lower panel) recorded from neurons inside day 35 hMLOs, evoked by current injection (the upper panel).
(E) The number of APs of neurons inside hMLOs that were generated in response to a particular current pulse. Error bars represent mean ± SEM (n = 12 and 14 for days 33–50 and 65–84, respectively).
(F) Spontaneous excitatory postsynaptic currents (sEPSCs) and spontaneous inhibitory postsynaptic currents (sIPSCs) (shown in 1) recorded from a neuron inside an hMLO at day 80. These sEPSCs and sIPSCs were blocked by CNQX (an AMPA-type glutamate receptor antagonist) and AP5 (an NMDA-type glutamate receptor antagonist) (shown in 2) and by picrotoxin (PTX, a GABAA blocker) (shown in 3).
(G) Electrical stimulation-evoked synaptic response recorded in the day 50 hMLO. The red dot indicates onset of electrical stimulation.
(H and I) Representative trace and frequency of spontaneous APs.
(J) Example traces of rebound depolarization. Insets show enlarged view of respective traces.
(K and L) Representative trace of pacemaker-like firing and the effect of quinpirole on firing frequency (K) and its statistical analysis (L). Error bars represent mean ± SEM (*p = 0.021, paired t test, n = 3).
(M) TH immunostaining of a neuron filled with biocytin during the recording, indicating that the recorded neuron expressed TH. Scale bar, 5 μm.
(N) DA measurement in hMLOs and hCOs by HPLC. Error bars represent mean ± SEM (hMLO 4w, 5w, 7w, and 9w [n = 4]; hMLO 13w; hCO 7w and 27w [n = 3]). See also Table S4.

cerebral organoids recapitulate gene expression programs of fetal neocortex development. Proc. Natl. Acad. Sci. USA *112*, 15672–15677.

Chambers, S.M., Fasano, C.A., Papapetrou, E.P., Tomishima, M., Sadelain, M., and Studer, L. (2009). Highly efficient neural conversion of human ES and iPS cells by dual inhibition of SMAD signaling. Nat. Biotechnol. *27*, 275–280.

Consortium, G.T.; GTEx Consortium (2015). Human genomics. The Genotype-Tissue Expression (GTEx) pilot analysis: multitissue gene regulation in humans. Science *348*, 648–660.

Fatehullah, A., Tan, S.H., and Barker, N. (2016). Organoids as an in vitro model of human development and disease. Nat. Cell Biol. *18*, 246–254.

Fedorow, H., Tribl, F., Halliday, G., Gerlach, M., Riederer, P., and Double, K.L. (2005). Neuromelanin in human dopamine neurons: comparison with peripheral melanins and relevance to Parkinson's disease. Prog. Neurobiol. *75*, 109–124.

Grealish, S., Diguet, E., Kirkeby, A., Mattsson, B., Heuer, A., Bramoulle, Y., Van Camp, N., Perrier, A.L., Hantraye, P., Björklund, A., and Parmar, M. (2014). Human ESC-derived dopamine neurons show similar preclinical efficacy and potency to fetal neurons when grafted in a rat model of Parkinson's disease. Cell Stem Cell *15*, 653–665.

Kelava, I., and Lancaster, M.A. (2016). Stem Cell Models of Human Brain Development. Cell Stem Cell *18*, 736–748.

Kim, D., Pertea, G., Trapnell, C., Pimentel, H., Kelley, R., and Salzberg, S.L. (2013). TopHat2: accurate alignment of transcriptomes in the presence of insertions, deletions and gene fusions. Genome Biol. *14*, R36.

Kirkeby, A., Grealish, S., Wolf, D.A., Nelander, J., Wood, J., Lundblad, M., Lindvall, O., and Parmar, M. (2012). Generation of regionally specified neural progenitors and functional neurons from human embryonic stem cells under defined conditions. Cell Rep. *1*, 703–714.

Korotkova, T.M., Ponomarenko, A.A., Brown, R.E., and Haas, H.L. (2004). Functional diversity of ventral midbrain dopamine and GABAergic neurons. Mol. Neurobiol. *29*, 243–259.

Kriks, S., Shim, J.W., Piao, J., Ganat, Y.M., Wakeman, D.R., Xie, Z., Carrillo-Reid, L., Auyeung, G., Antonacci, C., Buch, A., et al. (2011). Dopamine neurons derived from human ES cells efficiently engraft in animal models of Parkinson's disease. Nature *480*, 547–551.

Lancaster, M.A., Renner, M., Martin, C.A., Wenzel, D., Bicknell, L.S., Hurles, M.E., Homfray, T., Penninger, J.M., Jackson, A.P., and Knoblich, J.A. (2013). Cerebral organoids model human brain development and microcephaly. Nature *501*, 373–379.

Lawrence, M., Huber, W., Pagès, H., Aboyoun, P., Carlson, M., Gentleman, R., Morgan, M.T., and Carey, V.J. (2013). Software for computing and annotating genomic ranges. PLoS Comput. Biol. *9*, e1003118.

Lin, L., Göke, J., Cukuroglu, E., Dranias, M.R., VanDongen, A.M., and Stanton, L.W. (2016). Molecular Features Underlying Neurodegeneration Identified through In Vitro Modeling of Genetically Diverse Parkinson's Disease Patients. Cell Rep. *15*, 2411–2426.

Liu, H., and Zhang, S.C. (2011). Specification of neuronal and glial subtypes from human pluripotent stem cells. Cell. Mol. Life Sci. *68*, 3995–4008.

Love, M.I., Huber, W., and Anders, S. (2014). Moderated estimation of fold change and dispersion for RNA-seq data with DESeq2. Genome Biol. *15*, 550.

Mariani, J., Coppola, G., Zhang, P., Abyzov, A., Provini, L., Tomasini, L., Amenduni, M., Szekely, A., Palejev, D., Wilson, M., et al. (2015). FOXG1-Dependent Dysregulation of GABA/Glutamate Neuron Differentiation in Autism Spectrum Disorders. Cell *162*, 375–390.

Muguruma, K., Nishiyama, A., Kawakami, H., Hashimoto, K., and Sasai, Y. (2015). Self-organization of polarized cerebellar tissue in 3D culture of human pluripotent stem cells. Cell Rep. *10*, 537–550.

Paşca, A.M., Sloan, S.A., Clarke, L.E., Tian, Y., Makinson, C.D., Huber, N., Kim, C.H., Park, J.Y., O'Rourke, N.A., Nguyen, K.D., et al. (2015). Functional cortical neurons and astrocytes from human pluripotent stem cells in 3D culture. Nat. Methods *12*, 671–678.

Pfisterer, U., Kirkeby, A., Torper, O., Wood, J., Nelander, J., Dufour, A., Björklund, A., Lindvall, O., Jakobsson, J., and Parmar, M. (2011). Direct conversion of human fibroblasts to dopaminergic neurons. Proc. Natl. Acad. Sci. USA *108*, 10343–10348.

Poulin, J.F., Zou, J., Drouin-Ouellet, J., Kim, K.Y., Cicchetti, F., and Awatramani, R.B. (2014). Defining midbrain dopaminergic neuron diversity by single-cell gene expression profiling. Cell Rep. *9*, 930–943.

Qian, X., Nguyen, H.N., Song, M.M., Hadiono, C., Ogden, S.C., Hammack, C., Yao, B., Hamersky, G.R., Jacob, F., Zhong, C., et al. (2016). Brain-Region-Specific Organoids Using Mini-bioreactors for Modeling ZIKV Exposure. Cell *165*, 1238–1254.

Sasai, Y. (2013). Cytosystems dynamics in self-organization of tissue architecture. Nature *493*, 318–326.

Sasaki, H., Hui, C., Nakafuku, M., and Kondoh, H. (1997). A binding site for Gli proteins is essential for HNF-3beta floor plate enhancer activity in transgenics and can respond to Shh in vitro. Development *124*, 1313–1322.

Sulzer, D., Bogulavsky, J., Larsen, K.E., Behr, G., Karatekin, E., Kleinman, M.H., Turro, N., Krantz, D., Edwards, R.H., Greene, L.A., and Zecca, L. (2000). Neuromelanin biosynthesis is driven by excess cytosolic catecholamines not accumulated by synaptic vesicles. Proc. Natl. Acad. Sci. USA *97*, 11869–11874.

Yuan, Q., Yang, F., Xiao, Y., Tan, S., Husain, N., Ren, M., Hu, Z., Martinowich, K., Ng, J.S., Kim, P.J., et al. (2015). Regulation of Brain-Derived Neurotrophic Factor Exocytosis and Gamma-Aminobutyric Acidergic Interneuron Synapse by the Schizophrenia Susceptibility Gene Dysbindin-1. Biol. Psychiatry, in press. Published online August 28, 2015. http://dx.doi.org/10.1016/j.biopsych.2015.08.019.

Zecca, L., Zucca, F.A., Wilms, H., and Sulzer, D. (2003). Neuromelanin of the substantia nigra: a neuronal black hole with protective and toxic characteristics. Trends Neurosci. *26*, 578–580.

Zhang, W., Phillips, K., Wielgus, A.R., Liu, J., Albertini, A., Zucca, F.A., Faust, R., Qian, S.Y., Miller, D.S., Chignell, C.F., et al. (2011). Neuromelanin activates microglia and induces degeneration of dopaminergic neurons: implications for progression of Parkinson's disease. Neurotox. Res. *19*, 63–72.